Dewetting: Film Rupture by Nucleation in the Spinodal Regime

Uwe Thiele and Manuel G. Velarde
Instituto Pluridisciplinar, Universidad Complutense, Paseo Juan XXIII, 1, 28040 Madrid, Spain

Kai Neuffer
Instituto Pluridisciplinar, Universidad Complutense, Paseo Juan XXIII, 1, 28040 Madrid, Spain and Lehrstuhl für Statistische Physik and Nichtlineare Dynamik, BTU-Cottbus, Erich-Weinert-Strasse 1, 03046 Cottbus, Germany

(Received 21 December 2000; published 18 June 2001)

Unstable thin liquid films on solid substrates dewet by hole nucleation on defects or by a linear surface instability (spinodal dewetting). A system with destabilizing short-range and stabilizing long-range molecular interactions is investigated. We show that, for a subrange within the linearly unstable film thickness range, nucleation determines the final structure, whereas spinodal dewetting is of negligible influence. The results are also applicable to the spinodal decomposition of binary mixtures.

DOI: 10.1103/PhysRevLett.87.016104 PACS numbers: 68.15.+e, 47.20.Ma, 64.70.–p, 68.55.–a

The stability properties of thin liquid films on solid substrates are of technological importance in applications such as coating or drying processes. Film rupture can arise from surface tension stresses caused by temperature or surfactant concentration gradients and molecular interactions between the substrate and the film [1]. The latter may lead to dewetting for film thicknesses below 100 nm. Its study helps to develop methods to stabilize thin films [2] or to break thin films in a controlled manner [3]. Dewetting proceeds by the formation of holes, which subsequently grow laterally, resulting in polygonal networks of liquid rims or sets of liquid drops [4,5]. Investigations have focused on all aspects of the process: the rupture of the film [2,6], the growth process of single holes [7], the final overall pattern [5], and fingering instabilities during hole growth [8].

Film rupture proceeds by surface instability and hole nucleation on defects occurring in the ranges of linearly unstable and metastable film thicknesses, respectively [2,5,9]. Different methods have been employed to analyze the final pattern to identify the specific acting rupture mechanism. On the one hand, the agreement of the dependence of hole density on film thickness and the theoretical relation between the wavelength of the fastest growing linear mode and film thickness point towards dewetting by instability [5]. On the other hand, the order of arrangements of holes was measured to distinguish ordered (instability) and disordered (nucleation) patterns [9].

We think that part of the ambiguity of the results is caused by the prevailing belief that dewetting by instability dominates in the linearly unstable film thickness range, and hole nucleation at defects dominates outside this range. But we show here that, within the linearly unstable range, one has to distinguish instability-dominated and nucleation-dominated subranges.

The description of dewetting takes advantage of the disparity of length scales between film thickness and lateral changes in the film profile, allowing one to apply the long-wave approximation to the Stokes equations [1]. The resulting nonlinear evolution equation for the film thickness has the same functional form as the Cahn-Hillard equation describing the spinodal decomposition of a binary mixture [10]. Therefore dewetting by instability is also called "spinodal dewetting" [11]. The evolution equation reads

$$\partial_t h = -\partial_x\{Q(h)\partial_x[\gamma\partial_{xx}h + \Pi(h)]\}, \qquad (1)$$

where $h(x,t)$ is the film thickness, γ is the surface tension, $Q(h) = h^3/3\eta$ is the mobility factor due to Poiseuille flow, and η is the dynamic shear viscosity. The molecular forces are included through an additional pressure term, the disjoining pressure, $\Pi(h) = -\partial_h f(h)$, where $f(h)$ is a free energy. Here we use a combination of polar short-range destabilizing and apolar (Lifshitz–Van der Waals) long-range stabilizing interactions that is widely used in the literature [12]

$$\Pi(h) = 2S_{ap}\,\frac{d_0^2}{h^3} + \frac{S_p}{l}\,e^{(d_0-h)/l}. \qquad (2)$$

$d_0 = 0.158$ nm is the Born repulsion length and l is the correlation length of a polar fluid [13]. $S_P < 0$ and $S_{AP} > 0$ are the polar and apolar components of the total spreading coefficient, $S = S_{AP} + S_P$. However, the results are also qualitatively valid for other *formally* similar disjoining pressures and for spinodal decomposition [14]. Introducing the parameters $\kappa = (|S_p|/l)\exp(d_0/l)$ and $b = (2S_{ap}d_0^2/|S_p|l^2)\exp(-d_0/l)$ and using new scales $t = (3\eta\gamma/\kappa^2 l)\tilde{t}$ for time, $h = l\tilde{h}$ for film thickness, and $x = \sqrt{l\gamma/\kappa}\,\tilde{x}$ for the lateral coordinate, we obtain, after dropping the tildes, the dimensionless film evolution equation:

$$\partial_t h = -\partial_x\{h^3\partial_x[\partial_{xx}h - \partial_h f(h)]\}, \qquad (3)$$

with

$$f(h) = \frac{b}{2h^2} - e^{-h}. \qquad (4)$$

 © 2001 The American Physical Society

To assign an energy to every film profile $h(x,t)$, one uses the Lyapunov functional [14]

$$F(h) = \int \left[\frac{1}{2} (\partial_x h)^2 + f(h) - C_1(h - \overline{h}) \right] dx , \quad (5)$$

where $\overline{h}$ is the mean thickness and C_1 is the Lagrange multiplier corresponding to mass conservation. Minimizing the functional gives the equation describing stationary solutions,

$$0 = \partial_{xx} h(x) - \partial_h f(h) + C_1 . \quad (6)$$

It is also obtained by integrating Eq. (3) with $\partial_t h = 0$. The choice $C_1 = \partial_h f|_{h_0}$ ensures that the flat film $h(x) = h_0$ is a solution of Eq. (6). For localized solutions, h_0 is the thickness at infinity, whereas for periodic solutions, h_0 is the thickness at the inflection point of the profiles.

Before solving Eq. (6) and discussing stationary solutions of Eq. (3) let us first examine the linear stability of the flat film. It is obtained by linearizing Eq. (3) with the ansatz $h(x) = h_0 + \epsilon \exp(\beta t + ikx)$. The growth rate, β, for perturbations of wave number, k, is

$$\beta = -h_0^3 k^2 (k^2 + \partial_{hh} f|_{h_0}) . \quad (7)$$

The film is unstable for $\beta > 0$, i.e., for $\partial_{hh} f|_{h_0} < 0$ giving the unstable thickness range $h_i^d < h_0 < h_i^u$. At $b_c = 256/3e^4 \approx 1.56$ and $h_c = 4$ we find a critical point, i.e., for $b > b_c$ the films are always linearly stable. At $b = 0$ no upper instability limit exists and the lower limit scales as $h_i^d = (3b)^{1/4}$. The smallest unstable wavelength for a given h_0 is

$$\lambda_c = 2\pi(-\partial_{hh} f|_{h_0})^{-1/2}, \quad (8)$$

whereas the fastest growing mode has the wavelength $\lambda_m = \sqrt{2}\,\lambda_c$ with growth rate $\beta_m = h_0^3(\partial_{hh} f|_{h_0})^2/4$.

However, the absolute stability of a linearly stable film remains to be determined because it may be unstable to finite perturbations. To discuss this issue we assume an infinitely long film of thickness h_0 and give a small part of it (finite length L) the thickness h, hence ensuring that the mean film thickness remains h_0. The width of the transition region between the two levels is small compared to L, allowing one to neglect the gradient part of the energy (5). The energy per length of the disturbed part $g(h) = f(h) - C_1(h_0)h$ is shown in Fig. 1. We obtain (a) a single-well and (b) a generally asymmetric, double-well potential for $b < 8/e^2$ and $b_c > b > 8/e^2 = 1.08$, respectively. Minima represent linearly stable thicknesses, whereas only the deepest minimum represents an absolutely stable film. The other minimum is metastable. The maximum represents the linearly unstable film. For every b the metastable thickness range is limited by the h_0 allowing for two minima of equal depth. For $b > 8/e^2$ there exists an upper and a lower limit, denoted by h_m^u and h_m^d and characterized by $\partial_h f|_{h_m^u} = \partial_h f|_{h_m^d}$ and $g(h_m^u) = g(h_m^d)$. Note, h_m^u and h_m^d are also the equilibrium film thicknesses resulting from film decomposition after infinite time [11]. If $b < 8/e^2$ no upper limit of the metastable range exists and the lower limit is given by $\partial_h f|_{h_m^d} = 0$, securing $g(h \to \infty) = 0$. For $b \to 0$ the lower limit approaches zero as $h_m^d = b^{1/3}$. Linearly unstable and metastable thickness ranges are shown below in Fig. 4.

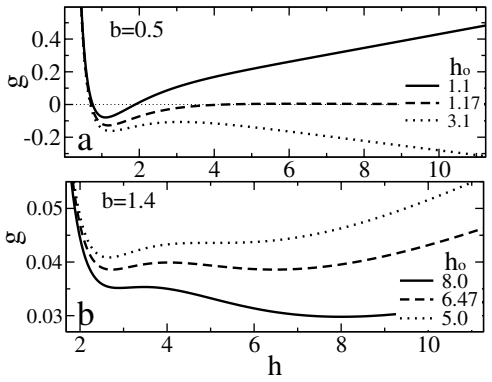

FIG. 1. The energy g for (a) $b = 0.5$ and (b) $b = 1.4$ and different film thicknesses, h_0. The respective dashed lines are for the h_0, giving the outer border of the metastable range.

Now we analyze the periodic solutions of Eq. (6) following [14]. By studying their energy and amplitude as a function of period for different fixed $\overline{h}$, we distinguish three different regimes (Fig. 2).

(i) The flat film is linearly unstable. One branch of periodic solutions exists, continuing towards infinite period. The energy, always lower than for the flat film, decreases and the amplitude increases monotonically with increasing period. The solutions are stable to disturbances of their period but unstable to coarse graining [14].

(ii) The flat film is linearly unstable. Two branches of periodic solutions exist, the low-energy branch with properties as (i) and the high-energy branch ending at the smallest unstable wavelength for the flat film, λ_c [Eq. (8)]. The latter branch has higher energy than the flat film and represents nucleation solutions as was confirmed by direct integration of Eq. (3) with different initial disturbances.

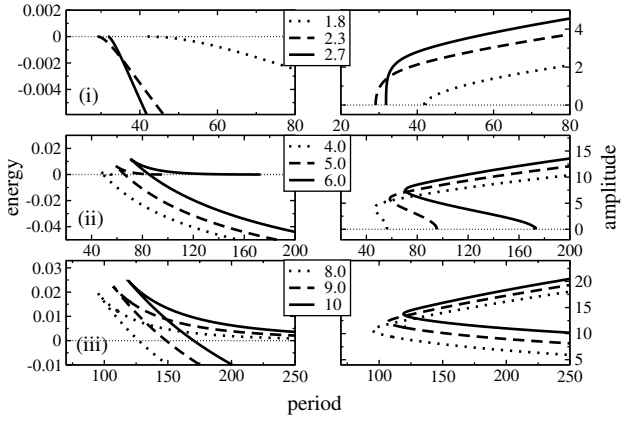

FIG. 2. Details of branches of periodic solutions for mean film thicknesses, $\overline{h}$, as shown in the insets at fixed $b = 0.5$. Shown are (left) energy-period and (right) amplitude-period dependencies. The energies are relative to the respective flat film energies.

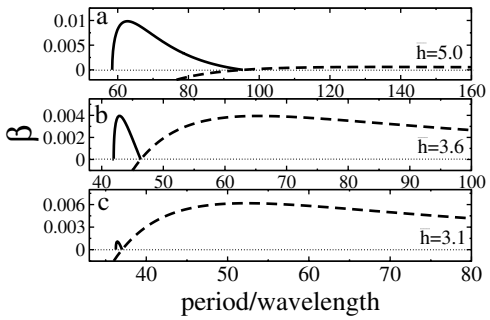

FIG. 3. Dependence of the linear growth rate of disturbances, β, on the period for nucleation solutions (solid lines) and on the wavelength for flat film solutions (dashed lines) for different values of $\overline{h}$ with $b = 0.5$.

If the disturbance amplitude is smaller than the amplitude of the respective nucleation solution the film flattens, whereas the disturbance grows if its amplitude is larger. The amplitude of the nucleation solutions increases with decreasing period.

(iii) The flat film is metastable. Two branches of periodic solutions exist. The low-energy branch has properties as (i) and the high-energy branch represents nucleation solutions of different periods as in (ii), but continues towards infinite period. The infinite period solution is a single critical hole, as found in wetting transitions [15].

The occurrence of nucleation solutions in (ii) implies that the distinction between instability range and nucleation range of the film thickness generally used in the literature has to be modified to accommodate three rather than two ranges: (i) instability range, (ii) range of mixed behavior, and (iii) nucleation range. To determine what will actually happen during the rupture process in the range of mixed behavior we perform a linear stability analysis on the nucleation solutions in (ii), $h_0(x)$, taking the ansatz $h(x) = h_0(x) + \epsilon h_1(x)e^{\beta t}$ [14].

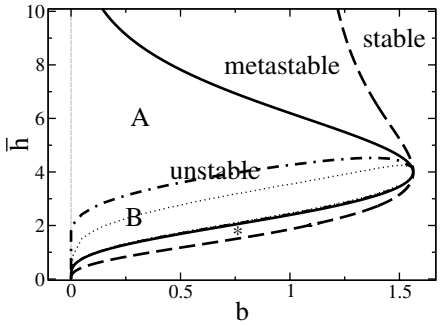

FIG. 4. The rupture regimes are shown within the parameter plane $(b, \overline{h})$. A and B denote, respectively, the nucleation-dominated and instability-dominated subranges within the linearly unstable thickness range (to the left of the solid line). They are separated by the dot-dashed line. The dotted line is the border between (i) the instability range and (ii) the range of mixed behavior. The star denotes the lower metastable range.

In Fig. 3 we compare the respective linear growth rates, β, of disturbances to the nucleation solutions and to the flat film [the latter obtained with Eq. (7)]. Depending on the mean film thickness, the maximal growth rate for the nucleation solutions can be much higher [Fig. 3(a)] or much lower [Fig. 3(c)] than for flat films, thus implying the physical importance of nucleation solutions down to small amplitude if the situation of Fig. 3(a) is given.

Taking this result as a hint of the local structure of the flow, $\partial_t h$, leads us to the assumption that there exists a nucleation-dominated subrange in the linearly unstable film thickness range, where local finite disturbances of a lateral extension comparable to the period of the above nucleation solutions have a crucial influence on the structure formation. However, they play a negligible role in the remaining instability-dominated subrange. We use the linear stability results to mark a border between nucleation-dominated and instability-dominated behavior at the film thickness, where both maximal growth rates are equal, as shown in Fig. 3(b). The numerically calculated values are represented by the dot-dashed line in Fig. 4.

To substantiate our assumption we integrate the evolution equation (3) for a system of size $L = n\lambda_m$, where $n > 1$ is an integer, taking as an initial condition a flat film with a localized disturbance, $h_{\text{init}} = \overline{h}\,[1 - d\,\cosh^{-2}(x/w\lambda_m)]$ of maximum depth, d, and width, w, in terms of the wavelength of the fastest flat film mode, λ_m. Calculating the time evolution for many different initial disturbances yields a clear qualitative distinction between the two subranges, as shown in Fig. 5.

(A) *Nucleation dominated.*—The disturbance grows, forming a hole with rims at its sides. This hole then expands laterally. Eventually, the thickness depressions at the outer base of the rims lead to secondary nucleation events [Fig. 5(a)]. The final, short-time structure (before coarse graining sets in) is a set of holes with distances not correlated with λ_m [last image of Fig. 5(a)]. However, it depends strongly on the initial disturbance, as can be seen in the evolution of the spatially averaged energy

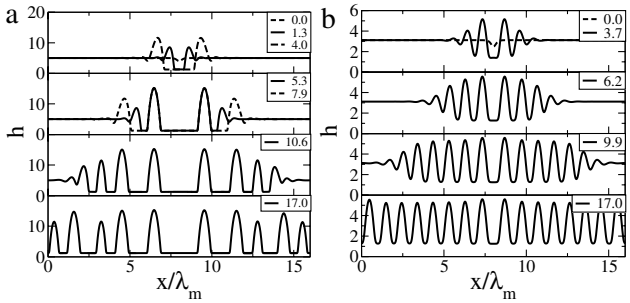

FIG. 5. Drastic difference in the short-time evolution of a localized disturbance between (a) nucleation-dominated subrange at $\overline{h} = 5.0$ and (b) instability-dominated subrange at $\overline{h} = 3.1$; both flat film thicknesses are linearly unstable. Parameter values: $b = 0.5$, $d = 0.2$, and $w = 0.2$. The insets show the corresponding times in units $\tau_m = 1/\beta_m$.

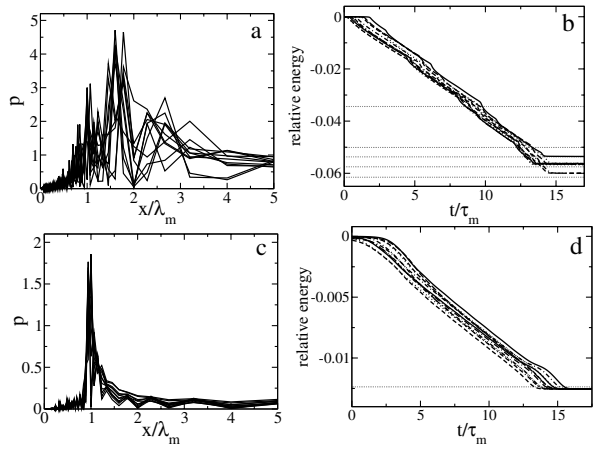

FIG. 6. Fourier transforms of the final short-time patterns at $t/\tau_m = 17.0$ for (a) $\overline{h} = 5.0$ and for (c) $\overline{h} = 3.1$. Average energy relative to the flat film for the short-time evolution for (b) $\overline{h} = 5.0$ and (d) $\overline{h} = 3.1$. The thin horizontal lines represent the energy for stationary solutions of periods (b) λ_m, $16\lambda_m/11$, $16\lambda_m/10$, $16\lambda_m/9$, $16\lambda_m/8$ (from above) and (d) λ_m. Shown are the results for eight different initial disturbances ($d = 0.1-0.3$, $w = 0.1-0.4$) at $b = 0.5$.

[Fig. 6(b)] and the Fourier spectrum of the final short-time structure [Fig. 6(a)] for different initial disturbances. We note that the energy even differs in its final short-time value.

(B) *Instability dominated.*—The disturbance starts to grow as in (A) but causes from the very beginning the growth of undulations on its two sides. These growing undulations have a period corresponding to the wavelength of the most unstable flat film mode and expand laterally [Fig. 5(b)]. The final short-time structure is a nearly periodic set of holes independent of the details of the initial disturbance, as shown in the Fourier spectra of a set of final structures in Fig. 6(c). The evolution of the energy [Fig. 6(d)] shows that only the very early phase of the process depends on the initial disturbance. Consequently, the evolution is nearly identical, only slightly shifted in time. In contrast to case (A), all final short-time structures have equal energy corresponding to the energy of the low-energy stationary solution of period λ_m.

We have analyzed the evolution of a thin liquid film under the influence of antagonistic long- and short-range interactions by determining the stable, metastable, and linearly unstable thickness ranges for flat films. We have found the branches of stationary solutions and have studied their linear stability. Thus, we have shown that the linearly unstable film thickness range comprises nucleation-dominated and instability-dominated subranges whose difference in time evolution has been seen by numerically integrating the evolution equation. In the nucleation-dominated subrange, initial finite disturbances are crucial for the final short-time structure, whereas the flat film modes are too slow to come into play. However, in the instability-dominated subrange the fastest growing flat film mode dominates while finite disturbances have negligible influence. These results hopefully help further understanding of the available experimental results [5,9]. Finally, we point out that by replacing the film thickness with concentration our findings can be transferred verbatim to spinodal decomposition and can be used to extend existing results on solution types and the transition between spinodal and nucleation dynamics in spinodal decomposition [16].

This work was supported by the European Union under ICOPAC Grant No. HPRN-CT-2000-00136, by the German Academic Exchange Board (DAAD) under Grant No. D/98/14745, and by the Spanish Ministry of Education and Culture under Grant No. PB 96-599.

[1] A. Oron, S. H. Davis, and S. G. Bankoff, Rev. Mod. Phys. **69**, 931 (1997).
[2] H. S. Kheshgi and L. E. Scriven, Chem. Eng. Sci. **46**, 519 (1991).
[3] M. Mertig, U. Thiele, J. Bradt, D. Klemm, and W. Pompe, Appl. Phys. A **66**, S565 (1998).
[4] F. Brochard-Wyart and J. Daillant, Can. J. Phys. **68**, 1084 (1989).
[5] G. Reiter, Phys. Rev. Lett. **68**, 75 (1992); R. Khanna, A. Sharma, and G. Reiter, Eur. Phys. J. Direct **E2**, 1 (2000).
[6] E. Ruckenstein and R. Jain, J. Chem. Soc. Faraday Trans. 2 **70**, 132 (1974).
[7] C. Redon, F. Brochard-Wyart, and F. Rondelez, Phys. Rev. Lett. **66**, 715 (1991); K. Jacobs, R. Seemann, G. Schatz, and S. Herminghaus, Langmuir **14**, 4961 (1998).
[8] N. Samid-Merzel, S. Lipson, and D. S. Tannhauser, Phys. Rev. E **57**, 2906 (1998).
[9] J. Bischof, D. Scherer, S. Herminghaus, and P. Leiderer, Phys. Rev. Lett. **77**, 1536 (1996); K. Jacobs, S. Herminghaus, and K. R. Mecke, Langmuir **14**, 965 (1998); U. Thiele, M. Mertig, and W. Pompe, Phys. Rev. Lett. **80**, 2869 (1998); H. I. Kim, C. M. Mate, K. A. Hannibal, and S. S. Perry, Phys. Rev. Lett. **82**, 3496 (1999).
[10] J. W. Cahn and J. W. Hillard, J. Chem. Phys. **28**, 258 (1958).
[11] V. S. Mitlin, J. Colloid Interface Sci. **156**, 491 (1993).
[12] B. V. Derjaguin, N. V. Churaev, and V. M. Muller, *Surface Forces* (Consultants Bureau, New York, 1987); J. N. Israelachvili, *Intermolecular and Surface Forces* (Academic Press, London, 1992); A. Sharma and R. Khanna, Phys. Rev. Lett. **81**, 3463 (1998).
[13] A. Sharma, Langmuir **9**, 861 (1993).
[14] U. Thiele, M. Velarde, K. Neuffer, and Y. Pomeau, Phys. Rev. E (to be published).
[15] R. Bausch, R. Blossey, and M. Burschka, J. Phys. A **27**, 1405 (1994).
[16] A. Novick-Cohen and L. A. Segel, Physica (Amsterdam) **10D**, 277 (1984); M. Hentschel, M. Bobeth, G. Diener, and W. Pompe, Thin Solid Films **354**, 267 (1999).